

All-optical three-dimensional electron momentum imaging

Emmanuel Orunesajo¹, Gihan Basnayake¹, Yasashri Ranathunga¹, Gabriel Stewart¹, David Heathcote², Claire Vallance², Suk Kyoung Lee¹ and Wen Li^{1*}

¹Department of Chemistry, Wayne State University, Detroit, MI, USA, 48202

²Department of Chemistry, University of Oxford, Chemistry Research Laboratory, 12 Mansfield Rd, Oxford OX1 3TA, UK

*corresponding author E-mail: wli@chem.wayne.edu

Abstract

We report a new implementation of three-dimensional (3D) momentum imaging for electrons, employing a two-dimensional (2D) imaging detector and a silicon photomultiplier tube (siPMT). In order to achieve the necessary time resolution for 3D electron imaging, a polyparaphenylene-dye-based fast scintillator (Exalite 404) was used in the imaging detector instead of conventional phosphors. The system demonstrated an electron time-of-flight resolution comparable with that of electrical MCP pick-off (tens of picoseconds), while achieving an unprecedented dead time reduction (~ 0.48 ns) when detecting two electrons.

Introduction

3D momentum imaging measures the momentum vectors of product fragments arising for photoionization/dissociation events and thus provides kinetically complete information to help resolve complex dynamics. Such measurements are achieved using a time- and position-sensitive detectors such as a delay-line detector¹⁻². The detectors measure the arrival time t and the positions (x,y) of each fragment after it has passed through an ion/electron spectrometer and these parameters are then used to reconstruct the momentum vectors of the fragment at its point of formation. Another powerful but indirect 3D momentum imaging method is Velocity Map Imaging (VMI)³, which was derived from the earlier approach of ion imaging⁴. In this method, the 3D Newton spheres of fragments are projected onto a 2D imaging detector and a mathematical inversion was used to retrieve the 3D momentum distributions⁵⁻⁷.

Li and coworkers recently developed a direct 3D-VMI system, in which a 2D imaging detector - comprising a pair of microchannel plates (MCP) coupled to a scintillator screen- and a camera are combined with a coincidence measurement of the arrival time by a digitizer to yield the needed time and space information (t,x,y) ⁸⁻¹⁰ of each event. The timing signal was picked-off either from the MCP high voltage inputs using capacitive decoupling or from a photomultiplier tube (PMT) that registers the flashes of light arising from a single electron/ion impact. In either case, the signal is passed through a digitizer in order to extract accurate arrival times. The hybrid detection method (camera+MCP pick-off) has so far yielded the best reported time resolution (~ 30 picoseconds)⁹ and the shortest deadtime (0.64 ns)¹⁰ when detecting two electrons in coincidence. While the all-optical approach (camera+PMT) is easy to implement, the achieved time resolution is limited to ~ 1 nanosecond due to the slow rise time (a few ns) and the long decay time (100 ns) of typically used phosphors (e. g. P47) in a 2D imaging detector. This time resolution is good

enough for 3D momentum imaging of ions, but it is not sufficient for electron 3D imaging or slice imaging. A previous study reported an ion time-of-flight (TOF) resolution of 100 ps with a multi-anode PMT and P20 phosphor while no electron TOF measurement was carried out¹¹.

Even though the hybrid detection method gives the best time-of-flight (TOF) resolution, it also has a few shortcomings. Firstly, because of the impedance mismatch between the detector assembly and the pick-off circuit, there is significant ringing in the acquired waveforms. The ringing distorts the waveform and increases the rise time and the width of the electrical pulses, which reduces the best possible time resolution and deadtime. Secondly, in VMI experiments, one often desires to pulse the MCP in order to selectively detect certain fragments or to implement ion-electron coincidence with a single detector¹². In this case, the high voltage pulses are likely to transmit via capacitive coupling to the processing circuits, potentially causing damage. Lastly, in 3D-VMI, when there are more than one hit registered, the brightness of the camera flashes and the signal peak height from the digitizer are used to correlate the positions (x,y) and arrival times (t) of each event^{8, 13}. This correlation might not be ideal due to the inhomogeneity of the phosphor screen in hybrid detection. This is because the MCP signals is proportional to the gain while the electron spot brightness seen by the camera depends on both the gain and the electron-to-photon conversion efficiency of the phosphor screen, which might not be uniform across the whole detector area^{8, 14}. All-optical detections can avoid these issues and allow much more flexible and simpler experimental configurations. However, can the all-optical detection ever achieve a high enough TOF resolution to be suitable for 3D electron momentum imaging? Recently, Vallance and coworkers reported that the organic dye Exalite 404 has much faster timing characteristics than P47 and its electron-to-photon conversion efficiency (brightness) is much higher than that of plastic scintillators, which also have good timing performance. These favorable properties make Exalite 404 a viable high-performing alternative to conventional phosphor materials and thus suitable to use with VMI and Pixel Imaging Mass Spectroscopy (PIMMS)¹⁵. The best demonstrated time resolution in ion TOF detection and imaging is about 2 ns¹⁶. In the following, we show that by employing this new scintillator together with a fast siPMT, the all-optical detection implemented in 3D-VMI can achieve comparable TOF resolutions with that of a hybrid detection (tens of picoseconds) and demonstrates a better deadtime when detecting multiple electrons.

Experimental Methods

The experimental setup including the vacuum chambers, the laser system and the ion/electron spectrometer has been described in detail previously¹⁷. We will focus mainly on the 3D momentum imaging system for electrons. The 2D imaging detector was a custom 75mm diameter dual-MCP detector (Beam Imaging System BOS-75). The original phosphor screen was coated with P47. In this experiment, the phosphor screen was replaced with a glass substrate coated with Exalite 404. The screen was prepared in a custom-designed fabrication chamber by vacuum sublimation. 111.9 mg of Exalite 404 scintillator was placed on a heating block inside the chamber, and the ITO-coated glass substrate was mounted above the block on the underside of the chamber lid. The chamber was pumped down to a pressure of 0.12 mbar, and the hot plate was heated to 180 degrees Celsius in four increments, with intermediate temperatures of 32.4, 60.0, 144.0, and 180.0 degrees Celsius. At each increment, the pressure was allowed to return

to the baseline pressure before the temperature was increased further. After reaching 180 degree, the chamber was sealed (*i.e.* pumping was stopped), and the temperature was increased to 250 degrees. Heating was then stopped, and the chamber remained sealed during cooling. Under these conditions the scintillator sublimates from the surface of the hot plate and recrystallizes on the surface of the substrate. Measurements on previously prepared screens indicate a typical coating thickness of 200 microns. As noted above, the glass substrate was pre-coated with indium tin oxide (ITO), also with a thickness of 200 microns, to enable an electrical bias to be applied in order to accelerate electrons emerging from the back face of the MCPs towards the scintillator.

To test the detection system, photoelectrons were produced from argon gas using strong field ionization at 800 nm, with a laser intensity of $\sim 5 \times 10^{13}$ W/cm² from a Ti: Sapphire laser with a pulse duration of ~ 30 fs (KMLabs, Red Dragon). The photoelectrons were extracted from the interaction region by a velocity-mapping field before impinging on the front face of the microchannel-plate detector. The positions of electron impact on the detector were captured by a highly sensitive CMOS camera (Basler acA720-520um), which is synchronized with the laser running at 1 kHz. To capture the timing information, a siPMT (OnSemi MICROFC-SMA-30050-GEVB) was used. A siPMT was chosen to provide the best timing performance at an affordable cost. The C30050 siPMT was listed with a rise time of 0.6 ns and an output pulse FWHM of 1.5 ns. In this work, we measured its impulse response by detecting femtosecond pulses (~ 30 fs). The fast output connector of the siPMT was connected to a National Instrument high-speed digitizer (PXI-5185) with 50 ohms impedance. The siPMT signal was digitized without any pre-amplification. For a side-by-side comparison, we also picked the signal from the front MCP and passed it through a 200 \times pre-amplifier (Ortec VT120) before connecting it to the second channel of the same digitizer. The digitizer was run at a sampling rate of 6.25 GS/s, which corresponds to a time bin of 160 ps. However, as shown previously, the ultimate time resolution is not limited by the sampling rate of the digitizer as long as the oversampling condition is met and trigger jitters are suppressed⁹. The digitizer was also triggered by the laser and thus all three signals (camera frames, siPMT and MCP traces) are synchronized. The camera frames were processed in real-time and clusters of non-zero pixels were grouped according to connectivity and centroided to give the positions of electron hits¹⁸. The digitized waveforms were analyzed in real-time to produce the TOFs of electron hits. They were also saved to a computer hard drive for more detailed multi-hit analysis.

Results and Discussion

1. siPMT and Exalite 404 timing performance

Figure 1a shows a digitized siPMT waveform arising from detecting femtosecond pulses. Because the laser pulse is extremely short at 30 fs, the trace should reflect the inherent timing characteristics of the siPMT alone. The rise time is about 0.78 ns and the pulse FWHM about 1.19 ns, which are close to the manufacturer's specifications. We further measured a relative time delay between signals from a photodiode (trigger) and the siPMT. This should represent the best possible time resolution that can be achieved with the siPMT using our timing analysis method

(Fig. 1b). The standard deviation of the distribution amounts to around 20 ps, which suggests that the transient spread time (TTS) of the siPMT is outstanding and it will not be a limiting factor in achieving a good electron TOF resolution. This performance is better than a previously reported result¹⁹. Fig. 2a shows a single electron hit on the detector as recorded by the siPMT. The trace has a rise time of 1.22 ns and a pulse FWHM of 2.73 ns, which is the result of a convolution of the amplified electron pulses, siPMT impulse response, and Exalite 404 rise and decay time. The timing characteristics are among the best we have observed so far in 3D-VMI experiments, hybrid detections included. More importantly, the trace is free of ringing and has no significant after-pulses. Because amplified electron pulses arriving at the scintillator are short (around ten picoseconds TTS for typical MCPs) and the siPMT timing is known (Fig. 1a), the timing response of Exalite 404 upon electron excitation can now be deconvoluted (Fig. 2b). The rise time is about 1.12 ns while the FWHM is about 2.09 ns. These results are comparable with that of fast plastic scintillators (e. g. BC404). The obvious advantage of Exalite 404 over BC404 is its high electron-to-photon conversion efficiency¹⁵. Even though the observed brightness of Exalite 404 was not as high as that of P47, the camera was able to detect the scintillation spots on the detector. The timing performance of the various components used in the experiment are summarized in table 1.

Timing Parameters	SiPMT	Single electron event viewed by siPMT	Exalite 404 (by deconvolution)
FWHM (ns)	1.19	2.73	2.09
Rise time (ns)	0.78	1.22	1.12
Decay time (ns)	0.91	2.59	1.54

Table 1: Timing parameters for Exalite 404, SiPMT and single electron event viewed by a siPMT. The rise time is defined as the time difference between 10% and 90% of the peak height. The decay time was obtained as the time constant by fitting the falling edge of the trace with a single-exponential decay.

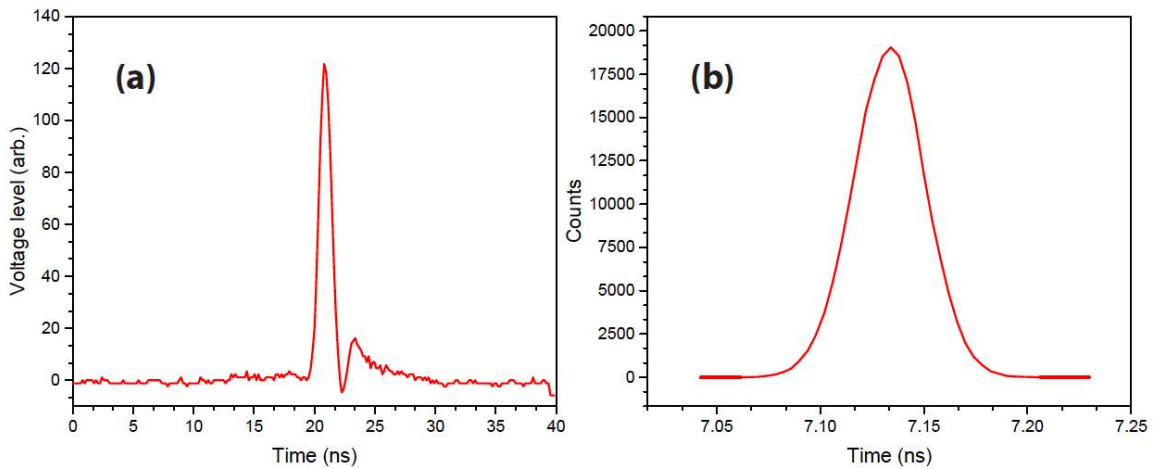


Fig. 1 Timing performance of the siPMT. (A) a single pulse siPMT trace generated by detecting a 30 fs laser pulse. (B) Relative time-delay of laser pulses measured between a trigger and the siPMT, showing a sub-sampling timing resolution, $\sigma=20$ ps.

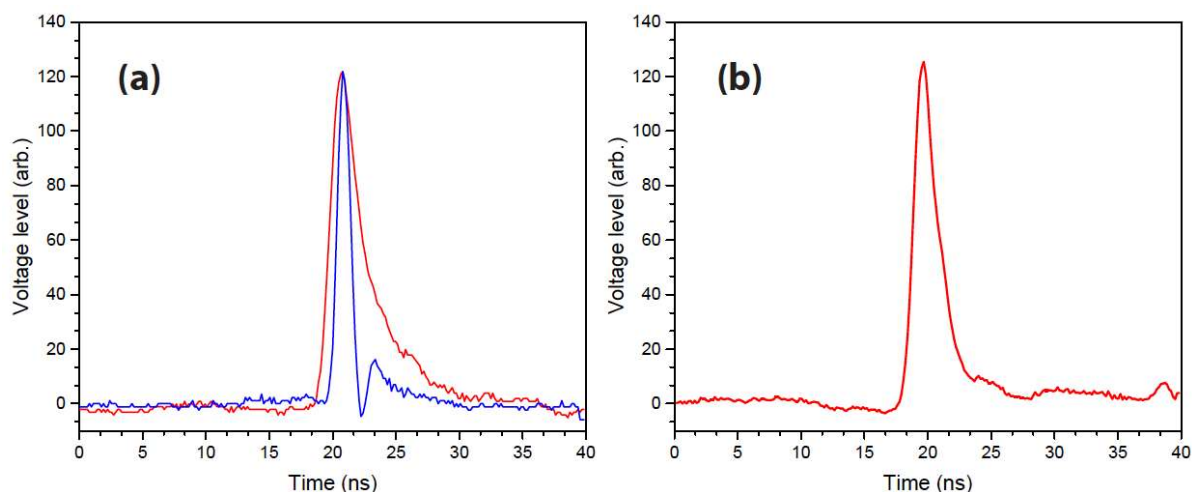


Fig. 2 The characterization of timing performance of Exalite 404 upon electron excitation. (A) digitizer waveforms arising from single electron event on the MCP/Exalite 404 screen (red) and a siPMT single pulse response (blue). The blue curve is the same as in Fig. 1a, replotted here for a direct comparison. (B) the deconvoluted Exalite 404 timing response.

2. 3D electron momentum imaging

In order to test the real-world performance of the all-optical electron imaging system, we detected electrons arising from above threshold ionization (ATI) in argon driven by a strong laser field.

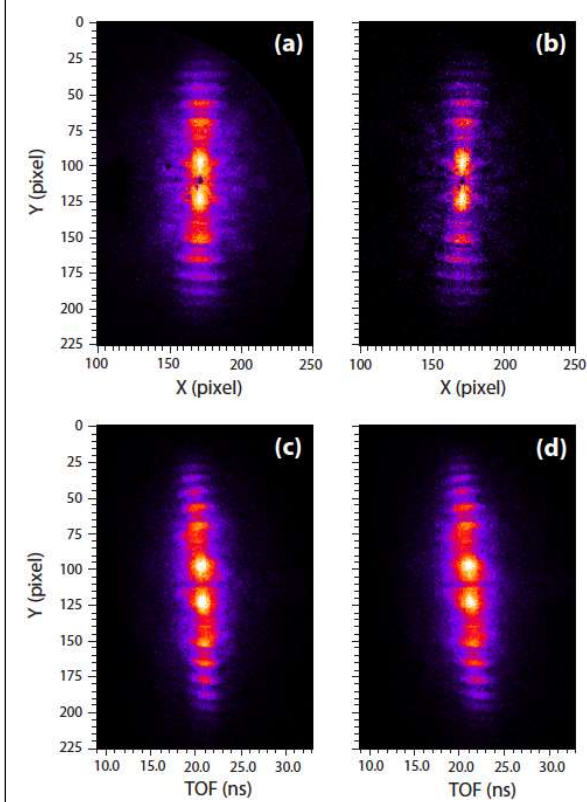
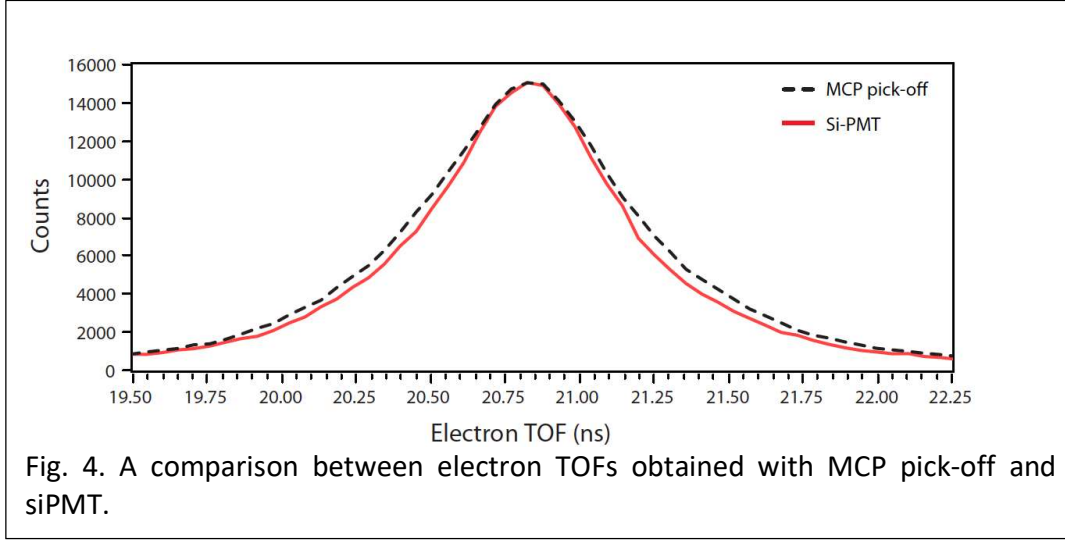


Fig. 3. 3D images of an electron Newton sphere. (A) X-Y image as viewed from a camera. (B) Sliced X-Y image. (C) Y-t image, in which t was obtained from the siPMT. (D) Y-t image, in which t was obtained by MCP pick-off.

In this process, an intense laser field interacts strongly with electrons in the atom and the electrons can absorb multiple photons beyond its ionization potential and gain a significant amount kinetic energy²⁰. 3D electron images obtained using both all-optical and hybrid detections are shown in Fig. 3. The TOFs of events were extracted by performing a peak detection algorithm on the obtained digitizer waveforms. The achieved time resolutions are comparable between these two methods. Figure 4 shows the overall TOF distributions, it seems the all-optical method even has a slightly smaller FWHM, suggesting a better time resolution. It should be noted that the electron TOF distribution has a FWHM of ~ 0.7 ns, which is quite challenging to resolve temporally. This is also the reason that the spatial images (x, y plane) shows more finely resolved details than spatial-temporal images (x, t plane). We estimated the TOF resolution obtained with the siPMT to be around 50 ps, which is somewhat worse than the best result achieved with hybrid detection (~ 32 ps). However, with this resolution, it is sufficient to time-slice (100 ps) the electron Newton sphere (Fig. 3b). The slight tilt in the Y-t image

(Fig. 3c and 3d) was the result of the laser polarization not being perfectly vertical. This was completely missing from the X-Y image (Fig. 3a), demonstrating the power of 3D imaging. It should be noted that we have observed previously that the time resolution achieved with hybrid detection can vary significantly from one detector to another due to different detector configurations and conditions. We expect the all-optical method to provide more consistent results since the pulse shape does not depend on specific detector configurations anymore. Instead, the timing performance of optical components such as scintillators and photon detectors become crucial, but they are relatively easy to adjust and improve.



3. Multi-hit detection

With a narrow FWHM having been demonstrated for each individual pulse in the all-optical method, we can expect a good multi-hit capability. The analysis methodology for multi-hit events is the same as that employed previously¹⁰: 1) An average single pulse waveform was produced by adding many scaled waveforms to improve the signal smoothness. 2) The average single pulse waveform was fitted with a sum of three gaussian functions with different widths and offsets to generate a basis function for resolving multi-hit events. 3) A least-square fitting using two basis functions was employed to fit the trace that arose from two coincident electron hit events. Such events could be easily identified by inspecting the electron hit counts from the corresponding camera frames. Figure 5a shows a 2D electron-electron TOFs distribution. Here, the diagonal line represents events for which the two TOFs cannot be resolved due to an extremely short time delay between two electrons. The shortest resolvable time difference is 0.48 ns, which is the best deadtime we have achieved so far. It should be noted that even though the TOFs are not fully resolved for those events on the diagonal line, these events are not lost, and this shows that the 3D-VMI method is essentially a zero-deadtime imaging system^{10, 21}. Furthermore, the correlation between the camera brightness and the digitizer peak height was quite good (Fig. 5b), which would facilitate the association between the position and TOF of each hit in a multi-hit event. Note under our current experimental condition, the two electrons observed in two-hit events arose from two separate ionization events in two different atoms, since the employed laser intensity was too low to produce double ionization events within a single atom. This provides a good test of the resolving power of the method: if the fitting algorithm works well, the overall

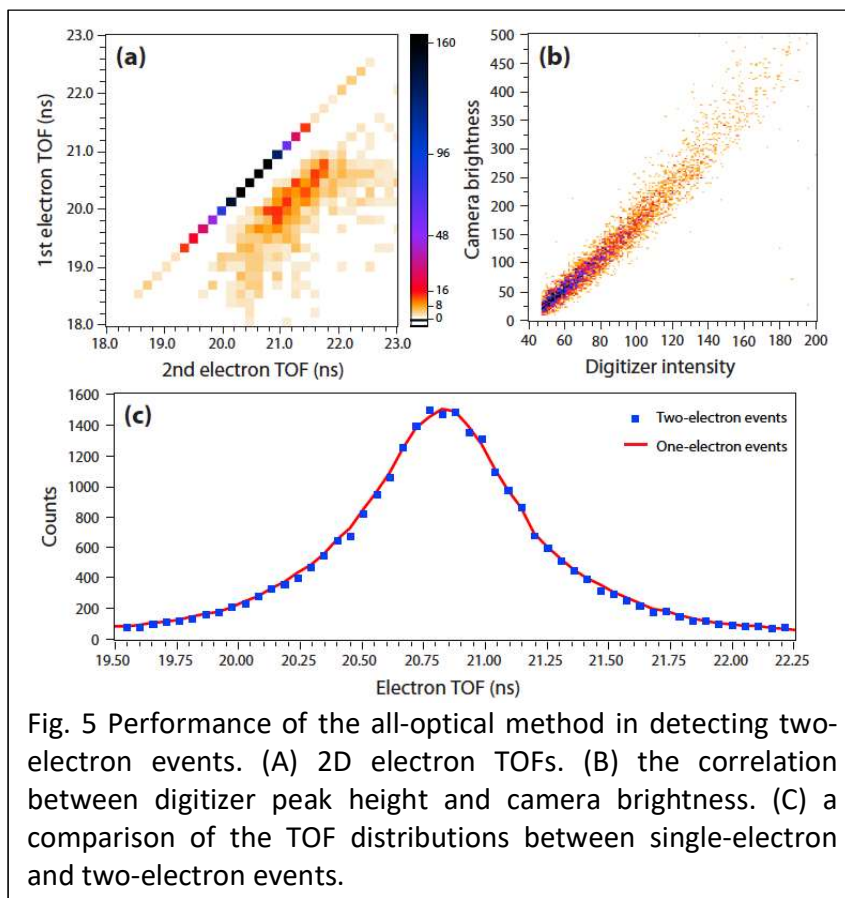


Fig. 5 Performance of the all-optical method in detecting two-electron events. (A) 2D electron TOFs. (B) the correlation between digitizer peak height and camera brightness. (C) a comparison of the TOF distributions between single-electron and two-electron events.

TOF distribution of the two-electron events should be exactly the same as that recorded for single electron events. This is indeed found to be the case, as shown in Fig. 5c that suggests the method does not introduce additional distortion to the resolved TOFs.

Conclusion

To summarize, by employing the all-optical detection implemented with a camera, a fast scintillator Exalite 404 and a siPMT, we have achieved some of the best performance of a 3D-VMI to date. The improved time resolution has enabled 3D electron imaging with

outstanding multi-hit capability when detecting two electrons. With the new setup, it is now possible to resolve three or more-hit events, which will be explored in future work. This will not only enable direct studies of multiple ionization dynamics²² but also increase the effective data rate of electron imaging experiments.

Acknowledgement:

Research supported by the U.S. Department of Energy (DOE), Office of Science, Basic Energy Sciences (BES), under Award # DE-SC0020994.

1. Ullrich, J.; Moshammer, R.; Dorn, A.; Dorner, R.; Schmidt, L. P. H.; Schiadt-Bocking, H., Recoil-Ion and Electron Momentum Spectroscopy: Reaction Microscopes. *Rep. Prog. Phys.* **2003**, *66*, 1463-1545.
2. Continetti, R. E., Coincidence Spectroscopy. *Ann. Rev. Phys. Chem.* **2001**, *52*, 165-192.
3. Eppink, A.; Parker, D., Velocity Map Imaging of Ions and Electrons Using Electrostatic Lenses: Application in Photoelectron and Photofragment Ion Imaging of Molecular Oxygen. *Rev. Sci. Instrum.* **1997**, *68*, 3477.
4. Chandler, D. W.; Houston, P. L., Two - Dimensional Imaging of State - Selected Photodissociation Products Detected by Multiphoton Ionization. *J. Chem. Phys.* **1987**, *87*, 1445-1447.

5. Heck, A. J. R.; Chandler, D. W., Imaging Techniques for the Study of Chemical Reaction Dynamics. *Ann. Rev. Phys. Chem.* **1995**, *46*, 335-372.
6. Bass, M. J.; Brouard, M.; Clark, A. P.; Vallance, C., Fourier Moment Analysis of Velocity-Map Ion Images. *J. Chem. Phys.* **2002**, *117*, 8723-8735.
7. Peter Rakitzis, T., Direct Measurement of Photofragment Alignment from Unnormalized Abel-Invertible Images. *Chem. Phys. Lett.* **2001**, *342*, 121-126.
8. Lee, S. K.; Cudry, F.; Lin, Y. F.; Lingenfelter, S.; Winney, A. H.; Fan, L.; Li, W., Coincidence Ion Imaging with a Fast Frame Camera. *Rev. Sci. Instrum.* **2014**, *85*, 123303.
9. Lee, S. K.; Lin, Y. F.; Lingenfelter, S.; Fan, L.; Winney, A. H.; Li, W., Communication: Time- and Space-Sliced Velocity Map Electron Imaging. *J. Chem. Phys.* **2014**, *141*, 221101.
10. Lin, Y. F.; Lee, S. K.; Adhikari, P.; Herath, T.; Lingenfelter, S.; Winney, A. H.; Li, W., Note: An Improved 3D Imaging System for Electron-Electron Coincidence Measurements. *Rev. Sci. Instrum.* **2015**, *86*, 096110.
11. Amitay, Z.; Zajfman, D., A New Type of Multiparticle Three-Dimensional Imaging Detector with Subnanosecond Time Resolution. *Rev. Sci. Instrum.* **1997**, *68*, 1387-1392.
12. Fan, L.; Lee, S. K.; Tu, Y.-J.; Mignolet, B.; Couch, D.; Dorney, K.; Nguyen, Q.; Wooldridge, L.; Murnane, M.; Remacle, F., et al., A New Electron-Ion Coincidence 3D Momentum-Imaging Method and Its Application in Probing Strong Field Dynamics of 2-Phenylethyl-N, N-Dimethylamine. *J. Chem. Phys.* **2017**, *147*, 013920.
13. Urbain, X.; Bech, D.; Van Roy, J.-P.; Géléoc, M.; Weber, S. J.; Huetz, A.; Picard, Y. J., A Zero Dead-Time Multi-Particle Time and Position Sensitive Detector Based on Correlation between Brightness and Amplitude. *Rev. Sci. Instrum.* **2015**, *86*, 023305.
14. Weeraratna, C.; Amarasinghe, C.; Lee, S. K.; Li, W.; Suits, A. G., Demonstration of Multi-Hit and Multi-Mass Capability of 3D Imaging in a Conventional Velocity Map Imaging Experiment. *J. Chem. Phys.* **2018**, *149*, 084202.
15. Winter, B.; King, S. J.; Brouard, M.; Vallance, C., A Fast Microchannel Plate-Scintillator Detector for Velocity Map Imaging and Imaging Mass Spectrometry. *Rev. Sci. Instrum.* **2014**, *85*, 023306.
16. Winter, B.; King, S. J.; Brouard, M.; Vallance, C., Improved Direct Detection of Low-Energy Ions Using a Multipixel Photon Counter Coupled with a Novel Scintillator. *Intl. J. Mass Spectrom.* **2016**, *397-398*, 27-31.
17. Winney, A. H.; Lee, S. K.; Lin, Y. F.; Liao, Q.; Adhikari, P.; Basnayake, G.; Schlegel, H. B.; Li, W., Attosecond Electron Correlation Dynamics in Double Ionization of Benzene Probed with Two-Electron Angular Streaking. *Phys. Rev. Lett.* **2017**, *119*, 123201.
18. Li, W.; Chambreau, S. D.; Lahankar, S. A.; Suits, A. G., Megapixel Ion Imaging with Standard Video. *Rev. Sci. Instrum.* **2005**, *76*, 063106.
19. Bonesini, M.; Bertoni, R.; de Bari, A.; Nardò, R.; Prata, M.; Rossella, M., Time of Flight Detectors with Sipmt Array Readout. *Nucl. Part. Phys. Proc.* **2016**, *273-275*, 1114-1120.
20. Yang, B.; Schafer, K. J.; Walker, B.; Kulander, K. C.; Agostini, P.; DiMauro, L. F., Intensity-Dependent Scattering Rings in High Order above-Threshold Ionization. *Phys. Rev. Lett.* **1993**, *71*, 3770-3773.
21. Liao, Q.; Winney, A. H.; Lee, S. K.; Lin, Y. F.; Adhikari, P.; Li, W., Coulomb-Repulsion-Assisted Double Ionization from Doubly Excited States of Argon. *Phys. Rev. A* **2017**, *96*, 023401.

22. Basnayake, G.; Fernando, S.; Stewart, G.; Debrah, D.; Lee, S. K.; Li, W., The Lack of Electron Momentum Correlation in Strong Field Triple Ionization of Molecules. *Mol. Phys.* **2021**, DOI: 10.1080/00268976.2021.1931722.

TOC Graphic

